

3-D DC resistivity modelling with arbitrary long electrode sources using finite element method on unstructured grids

Jun Yang, Yuanying Liu and Xiaoping Wu

Laboratory of Seismology and Physics of Earth's Interior, School of Earth and Space Sciences, University of Science and Technology of China, Hefei 230026, China. E-mail: wxp@ustc.edu.cn

Accepted 2017 August 21. Received 2017 August 18; in original form 2016 September 5

SUMMARY

We present a 3-D electrical resistivity modelling with long electrode sources using finite element method on unstructured tetrahedral grids. The radius and resistivity of the electrode is neglected and the electrode can be regarded as a line source with finite length in our modelling. An approximated equation for determining the current density along the electrode is derived for current density correction in heterogeneous media. Electrical fields excited by arbitrary long electrode sources in heterogeneous conductive media can be simulated. Both total- and secondary-potential methods are implemented in the simulation. The analytic electrical potentials of an arbitrary long electrode source in a conductive half-space is derived and used for accuracy analysis in the numerical simulations. The apparent resistivities for survey arrays with long electrode sources are proposed based on the analytic solution of the half-space model. The responses of electrical fields excited by point electrode and long electrode sources to resistivity anomalies are compared with ground and borehole simulations, which shows that the arrays with long electrode sources are more sensitive to the anomalies than those with point electrode sources. A time-lapsed monitoring for hydraulic fracturing in oil field using the production wells as long electrode sources is also simulated, which indicates that the borehole potential data of the long electrode source array can help assess the location of the fracture zone.

Key words: Electrical properties; Hydrogeophysics; Electromagnetic theory; Numerical solutions.

1 INTRODUCTION

Direct current (DC) electrical prospecting characterizes the near surface resistivity structure by injecting DC into the earth and measuring the electrical potential distribution with electrodes on the ground or in boreholes. It is widely used in civil engineering survey, environmental and hydraulic monitoring, geological investigation, mining exploration and other geophysical engineering, as well as agricultural applications (e.g. Daily *et al.* 1992; Maillol *et al.* 1999; Hauck 2002; Israel & Pachauri 2003; Rucker *et al.* 2009; Sudha *et al.* 2009; Beff *et al.* 2013; Johnson *et al.* 2015). Steel or brass stakes have been used for current injection and treated as point electrode (PE) sources in conventional electrical prospecting.

During the exploration and exploitation of solid minerals and hydrocarbons, wells will be drilled for observation and production. Once they are cased, the wells become good conductors and can be used as electrodes for current injection in electrical prospecting, which may be a new, attractive application for these wells, besides production. A cased well cannot be regarded as a PE due to their axial extension and we refer it as the long electrode (LE) source in this paper. Horizontal wells are often drilled in shale gas reservoir (Waters *et al.* 2009) and in the geological formations for CO₂ storage

(Byun *et al.* 2010). These multisectioned wells have more complicated geometries and the resistivity modelling with such DC sources are more challenging. In order to understand the electrical field excited by LE sources and investigate their capability to underground prospecting, we implement a 3-D DC resistivity modelling with LE sources. The LEs are not restricted to the cased wells. In fact, any good conductors in the shape of a finite line section can be used as LE sources, such as buried long wires, metallic pipes and rebars. For a steel casing, the resistivity can be as low as $2.3 \times 10^{-7} \Omega\text{m}$ (Pardo & Torres-Verdín 2013) which is several orders of magnitude smaller than the common earth media and thus can be neglected. The radius of the LE is negligible as well, compared with its length extent. LEs may have some advantages over PEs by virtue of their geometries. For one thing, the contact resistance of an LE is much smaller than that of a PE, which makes it easier to inject larger current into the earth. For another, the use of LEs as sources may also extend the prospecting depth in electrical resistivity surveys as they can deliver more current to deep formations.

It has long been known that LEs can be used in electrical prospecting. Rocroi & Koulikov (1985) investigated the use of steel casings for the prospecting of hydrocarbon. They found that the apparent resistivity profiles obtained using vertical casings as sources

are more sensitive to resistivity change in greater depth than those of the ground PEs. Ushijima *et al.* (1999) employed vertical casings for monitoring hydraulic fracturing and oil recovery process in reservoirs. Some approximated models have been proposed for the simulation of electrical field with LE sources. The most popular analog is the conductive cell model (CCM), which places a highly conductive column, energized by a PE, to represent the LE in the simulation model (Daily *et al.* 2004; Rucker *et al.* 2010, 2011; Rucker 2012; Weiss *et al.* 2016). The accuracy of the CCM solution will be affected by the resistivity of the column (Rucker *et al.* 2010). If very low resistivity is assigned to the column, the sharp resistivity contrast between the earth media and the electrode may result in convergence problem when solving the system of linear equations. Another strategy used in the numerical simulations is that the conductivity of the LE is assumed to be infinite, so that the electrode can be regarded as a perfect electrical conductor. Zhu & Feng (2011), Zhu (2012) conducted electrical resistivity tomography using a vertical LE on structured grids to assess the residual oil saturation, in which the LE was regarded as a line source. However, their simulation cannot handle arbitrary LE sources and the vertical LE source is restricted in a homogeneous region. Rücker & Günther (2011) probed the influence of the extent of the electrode on electrical field using the complete electrode model (CEM) which took into account the shape of the electrodes, but the apparent resistivity in their study is based on the point source solution. Zhang *et al.* (2014) reported the current density change at the bottom end of the LE and that the surface current density of the LE should not be constant in stratified formations. Ronczka *et al.* (2015) simulated the LE using a shunt electrode model (SEM), in which a set of discrete nodes connected by shunt conductors were used to mimic the highly conductive LE. They also evaluated the apparent resistivity of LE arrays using the numerical solutions. Johnson & Wellman (2015) applied an immersed interface method to simulate the electrical field of PE source with the presence of metallic infrastructures. However, intensive computation is required in their simulation as the computational domain is decomposed into background region and perfect conducting regions and the partial solutions need to be scaled using a divergence condition. In addition, a geometric representation of the LEs needs to be constructed in their simulation, the same as the simulations using CCM and CEM, which may bring in difficulty in mesh generation and increase the computational cost when the radius of the electrode is too small.

In this paper, we implement a new 3-D resistivity modelling with arbitrary LEs using finite element method (FEM), following the line source approximation presented by Zhu & Feng (2011). The arbitrariness of the LEs includes (1) arbitrary dips and azimuths and (2) arbitrarily multisectioned geometry. Unstructured tetrahedral meshes are employed for spatial discretization. Structured grids are often used for discretization as they can be generated in a simpler way, but they have difficulties handling complex geometries, irregular boundaries or topographies. Moreover, the elements near the boundary will be distorted severely when local refinements are conducted on structured grids. Unstructured grids, on the other hand, offer better geometric adaptability and local refinement can be done without interfering with the quality of the elements in other region. With our simulation scenario, no actual electrode structure is needed in the mesh model. Both total potential and secondary potential methods can be applied in the simulation. To handle the case of heterogeneous media, we derive an approximated equation for current density correction along the LE source. The analytic potential excited by a vertical line source in a half-space was given by Wait (1982) and Bhagwan & Troffimienoff (1982). We further de-

rive the analytic potential excited by an arbitrary LE in a conductive half-space model (see Appendix). The apparent resistivity formulas for LE arrays are also proposed based on the analytic solution of the half-space model. In the studies of Daily *et al.* (2004) and Rucker *et al.* (2010), LEs are used for both current injection and potential measurement. However, apparent resistivity is not available when LEs are used for potential measurement. Meanwhile, it results in a loss in vertical resolution (Daily *et al.* 2004). In our simulation, potentials are measured using PEs. Accordingly, an LE source array refers to an array with LE sources and PE receivers in this paper. The differences between LE and PE sources are discussed regarding the field pattern, apparent resistivity and sensitivity to underground anomalies. Finally, a hydraulic fracturing model is designed to test the capability of LE sources for monitoring the fracturing process in a horizontal well with time-lapsed data.

2 NUMERICAL SCHEME

2.1 The variational problem of LE electrical field

Similar to the problem of finite fault source in seismology (Beresnev & Atkinson 1997), discretization needs to be done to the LE source first and the discrete line elements are regarded as a series of PE sources. The electrical field of a PE in conductive media is governed by a Poisson equation with appropriate boundary conditions and the boundary value problem can be transformed to a variational problem, to which a finite element discretization can be applied (Zhou & Greenhalgh 2001; Li & Spitzer 2002; Wu 2003; Rücker *et al.* 2006; Wang *et al.* 2013). For our LE simulation, a line integral is imposed to the functional of the PE variational problem, which gives

$$F_L[u] = \int_L \left\{ \int_{\Omega} \left[\frac{1}{2} \sigma (\nabla u)^2 - u \nabla \cdot \mathbf{J}(\mathbf{r}_s) \right] dV + \frac{1}{2} \int_{\partial\Omega} \alpha \sigma u^2 dS \right\} dl, \quad \mathbf{r}_s \in L. \quad (1)$$

The square brackets in $F_L[u]$ denote a functional with respect to potential u . The surface integral term stands for the boundary condition, where α is a coefficient related to the domain boundary. On the surface boundary, α is set to be zero, while for the artificial truncated boundary, a mixed boundary condition is employed (Zhou & Greenhalgh 2001). In PE simulation, the source term $\nabla \cdot \mathbf{J}$ can be represented by a Dirac delta function at a fixed source point (Ward & Hohmann 1987; Rücker *et al.* 2006). However, when the LE penetrates through heterogeneous media, the current density on the LE surface varies with surrounding media, thus the current density \mathbf{J} is a function of \mathbf{r}_s , as shown in eq. (1). Consequently, $\nabla \cdot \mathbf{J}(\mathbf{r}_s)$ needs to be determined first in order to proceed with the numerical simulation.

2.2 The current density distribution along an LE source in heterogeneous media

In the study of Zhu & Feng (2011), the current density along the LE is assumed to be constant, thus the LE is restricted in homogeneous medium. When an LE source is inserted into heterogeneous media, the analytic current density distribution is not available. We will propose an approximated distribution for the current density along the source line for such cases in this section.

Let us consider the electrical field on the surface of an LE penetrating through an irregular resistivity anomaly (Fig. 1). Once the

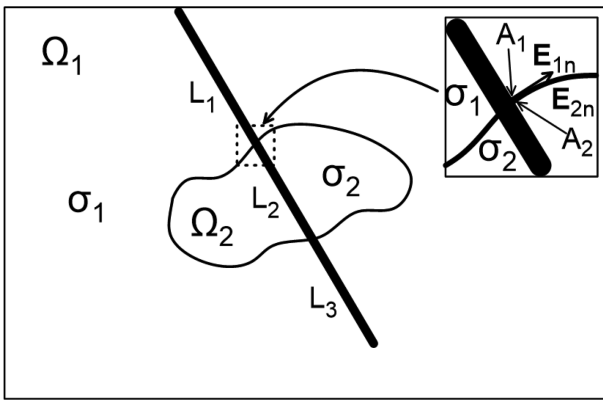


Figure 1. A simple model of LE source penetrating through heterogeneity. E_{1n} and E_{2n} denote the normal component of the electrical fields on the LE surface on both sides of the resistivity interface.

electrical field on the LE surface is determined, the current density distribution can be calculated by means of the Ohm's law

$$\mathbf{J} = \sigma \mathbf{E}. \quad (2)$$

Consequently, only the electrical field on the LE surface is of interest in the following discussion. In the line source model, the resistivity of the electrode is neglected, namely the electrode is a perfect electrical conductor and an equipotential body, which implies that there is no tangential electrical field on the LE surface and the electrical field in normal direction is uniform when an LE section is embedded in one homogeneous medium. In Fig. 1, We further assume that the interface between region Ω_1 and Ω_2 is perpendicular to the LE in close proximity to the intersecting points where the LE penetrates into Ω_2 from Ω_1 . This assumption is reasonable in the region that is extremely close to the LE surface. Then the electrical field normal to the LE surface is parallel to the resistivity interface. Denoted by A_1 and A_2 two points on the LE surface which locate extremely close to each other on both sides of the interface, the application of the tangential continuity of the electrical field in the interface leads to an equality of normal electrical field, $E_{1n} = E_{2n}$. Since the electrical fields are uniform in each section and there is no tangential electrical field on the LE surface, the following relation is obtained,

$$\mathbf{E}_1 = \mathbf{E}_2 = \mathbf{E}_3, \quad (3)$$

where \mathbf{E}_i is the electrical field intensity on the surface of the L_i section. As a result, the electrical field is uniform along the whole LE, regardless of the heterogeneous surrounding media. For the case that an LE is embedded in the interface of two layers, the same result can be obtained by applying the tangential continuity condition of the electrical field on both side of the interface. Since the LE is simplified as a line source with finite length, the current density at a certain point on the LE is actually infinity and we need to define the current density in a limit form. The total current strength of the LE with a radius of r can be calculated as

$$I = \int_{\Omega} \nabla \cdot \mathbf{J}(\mathbf{r}_s) dV = \int_{\partial\Omega} \mathbf{J}(\mathbf{r}_s) \cdot d\mathbf{S} = \int_L \int_0^{2\pi} \mathbf{J}(\mathbf{r}_s) \cdot \mathbf{r} d\theta dl. \quad (4)$$

Let $|\mathbf{r}| \rightarrow 0$,

$$I = \lim_{|\mathbf{r}| \rightarrow 0} \int_L J(\mathbf{r}_s) dl = \sum_{i=1}^3 J_i L_i, \quad (5)$$

where

$$J_i = \lim_{|\mathbf{r}| \rightarrow 0} \int_0^{2\pi} \mathbf{J}(\mathbf{r}_s) \cdot \mathbf{r} d\theta, \quad \mathbf{r}_s \in L_i, \quad (6)$$

can be regarded as the scalar current density of the i th LE section. According to Ohm's law (2) and (3), we arrive at a conclusion that the current density on the LE surface is proportional to the conductivity of the surrounding medium,

$$\frac{J_1}{\sigma_1} = \frac{J_2}{\sigma_2} = \frac{J_3}{\sigma_3}. \quad (7)$$

For a general case, when an LE penetrates through n resistivity blocks with total injection current I , the following equations hold,

$$I = \sum_{i=1}^n J_i L_i, \quad (8)$$

$$\frac{J_1}{\sigma_1} = \frac{J_2}{\sigma_2} = \dots = \frac{J_n}{\sigma_n} = m, \quad m \in \Re^+, \quad (9)$$

where σ_i is the conductivity of the block in which section L_i is embedded and J_i can be regarded as the line current strength density. Finally, the current strength density of the k th section is given as

$$J_k = \frac{\sigma_k I}{\sum_{i=1}^n \sigma_i L_i}, \quad (10)$$

which is denoted as the current density allocation (CDA) equation in this paper. The CDA equation is an approximated solution due to the simplified assumptions, but when the LE is highly conductive and the region of interest is not extremely close to the source line, this method provides a good approximation. The actual electrical fields, and thus current densities, do not only depend on the local conductivity but the whole conductivity distribution around. In this section, only the conductivity distribution close to the LE is taken into account because we focus on the electrical field on the LE surface and the derivation of the CDA equation is based on Ohm's law. This treatment is in some way transforming the source term into a boundary condition, which is similar to the transient electromagnetics simulation when the source term is replaced by an initial condition (the transient EM field at early time) (e.g. Wang & Hohmann 1993). We pre-calculate the 'boundary condition' using the CDA equation instead of coupling it into the linear system as CEM does. When the current on the LE surface spreads out into the conductive media, the current density will be adjusted by the conductivity distribution according to Ohm's Law. This procedure takes place in solving the system of linear equations, which is to be discussed in the next section, and our simulation results obey the physical laws.

2.3 The finite element scheme

Unstructured tetrahedral grids are used for spatial discretization in the simulation. Let \mathcal{T}_h be a discretization of the computational domain Ω . For each tetrahedral element $K \in \mathcal{T}_h$, the conductivity σ is assumed to be constant. A finite dimensional space of linear function defined on the element K by $\mathcal{P}_1(K)$ is chosen to approximate the solution,

$$\mathcal{P}_1(K) = \left\{ v : v = a_0 + \sum_{i=1}^3 a_i x_i, (x_1, x_2, x_3) \in K, a_i \in \Re \right\}. \quad (11)$$

By defining

$$V_h := \{v : v \in C^0(\Omega), v|_K \in \mathcal{P}_1(K) \quad \forall K \in \mathcal{T}_h\}, \quad (12)$$

the potential u within K can be approximated by a linear interpolation

$$\mathbf{u} = \sum_{i=1}^4 u_i \phi_i, \quad (13)$$

where $u_i \in V_h$ and $\phi_i \in \mathcal{P}_1(K)$ are the approximate solution at the i -th node of element K and the corresponding linear basis function (also known as shape functions), respectively. By substituting eq. (13) to functional (1), we obtain

$$F_L[u] = \sum_{\Omega} \left(\frac{1}{2} \mathbf{u}^T \mathbf{A} \mathbf{u} + \frac{1}{2} \mathbf{u}^T \mathbf{B} \mathbf{u} - \mathbf{u}^T \mathbf{p} \right), \quad (14)$$

where $\mathbf{u} = (u_1, u_2, u_3, u_4)^T$. The local matrices and source term vector are calculated as

$$\mathbf{A} = \int_L \sigma \int_K \boldsymbol{\phi} \boldsymbol{\phi}^T dV dl, \quad (15)$$

$$\mathbf{B} = \int_L \alpha \sigma \int_{\partial K} \nabla \boldsymbol{\phi} \cdot \nabla \boldsymbol{\phi}^T dS dl, \quad (16)$$

$$\mathbf{p} = \int_L \int_K \nabla \cdot \mathbf{J}(\mathbf{r}_s) \boldsymbol{\phi} dV dl, \quad (17)$$

where $\boldsymbol{\phi} = (\phi_1, \phi_2, \phi_3, \phi_4)^T$. The volume integral in (15) and the surface integral in (16) are usually called the mass matrix and the stiffness matrix, respectively. It is clear that $B_{ij} = 0$ on the surface boundary and eqs (15)–(17) hold for arbitrarily multisected LE sources. By taking the first variation of the discrete functional (14) and set the variation to be zero, a system of linear equations is obtained

$$\mathbf{Q}\mathbf{U} = \mathbf{P}, \quad (18)$$

where \mathbf{U} and \mathbf{P} are the total unknowns and global source term, respectively, and

$$\mathbf{Q} = \sum_{\Omega} (\mathbf{A} + \mathbf{B}), \quad (19)$$

is the global matrix, which is sparse, symmetric and positive definite.

2.4 Secondary potential method

The source term $\nabla \cdot \mathbf{J}(\mathbf{r}_s)$ in eq. (1) leads to a singularity at the source position. This singularity will severely deteriorate the accuracy of the numerical solution in source region. In order to remove the singularity of the source, Coggon (1971) and Lowry *et al.* (1989) suggested splitting up the total potential u into primary potential u_p and secondary potential u_s ,

$$u = u_p + u_s. \quad (20)$$

This singularity removal technique has been widely adopted in DC resistivity modelling later on (e.g. Zhao & Yedlin 1996; Li & Spitzer 2002; Wu 2003; Rücker *et al.* 2006; Wang *et al.* 2013). This method can also be applied to the LE simulation by substituting u with (20), which yields the variational problem with respect to u_s ,

$$F_L[u_s] = \int_L \left\{ \int_{\Omega} \left[\frac{1}{2} \sigma (\nabla u)^2 - \sigma_a \nabla u_p u_s \right] dV + \int_{\partial \Omega} \alpha \left(\frac{1}{2} \sigma u_s^2 - \sigma_a u_p u_s \right) dS \right\} dl, \quad (21)$$

where $\sigma_a = \sigma_p - \sigma$ is the anomalous conductivity and σ_p is the background conductivity corresponding to the primary potential u_p .

By repeating the same procedure as in Section 2.3, a system of linear equations with respect to u_s is obtained for LE source,

$$\mathbf{Q}\mathbf{U}_s = \mathbf{Q}'\mathbf{U}_p. \quad (22)$$

To calculate \mathbf{Q}' , the conductivity σ in (15) and (16) needs to be replaced by σ_a . The primary potential \mathbf{U}_p will be calculated analytically (see Appendix) and the singular source term vanishes. When the LE source penetrates through heterogeneous media, the simulation using secondary potential method becomes a little more complicated as a global primary potential is no longer available. In order to solve this problem, we divide the LE into subsections with each subsection embedded in one homogeneous block and each subsection is regarded as an independent LE source (Fig. 2). Then the current strength of each section is reallocated using the CDA equation (10) and the system of linear equations (22) for each LE section is solved. Finally, the total potential is obtained by summing up the solution of each section. FE algorithms of both total and secondary potential version have been implemented in our study and it is clear that total potential version algorithm will be preferred when the LE sources are embedded in highly heterogeneous media.

2.5 Solving the system of linear equations

Due to the sparsity and symmetry of the global matrix \mathbf{Q} , we only store the non-zero elements in the upper triangle portion of the matrix, according to the compressed row storage format which results in a striking decrease in memory demand in the forward modelling. The system of linear equations is solved using a conjugate gradient method with a symmetric successive over-relaxation pre-conditioner (SSOR-PCG; Spitzer 1995; Li & Spitzer 2002). A direct solver (Schenk & Gärtner 2004) is also tested for solving the system of linear equations. We find that the direct solver is superior in stability, especially for models with sharp resistivity contrast, but the iterative solver give the same solution with six significant digits. The reason that we prefer an iterative solver is that the direct solver has a much higher memory demand. A system of linear equations with about 200 000 unknowns can be solved by the iterative solver on a laptop with 2 GB memory, but it crashes when the direct solver is applied.

3 ACCURACY OF THE FE SOLUTIONS

3.1 A homogeneous half-space model for total-potential method

As shown in Fig. 3(a), a 100 Ωm homogeneous half-space model with a three-sectioned LE source embedded in it is used for validating the total-potential-version FE algorithm. The calculation domain is a cylinder with a radius and depth extent of 1000 m. Two survey lines are set with S1 on the ground along x -axis and S2 in a borehole. A non-commercial mesh generator, Gmsh (Geuzaine & Remacle 2009), is employed for generating unstructured tetrahedral meshes in our study. A total of 196 481 tetrahedra with 38 179 vertices are generated in this model. Local refinement is applied in the vicinity of the source and the survey lines (Fig. 3b).

The potential profiles along survey lines S1 and S2 (Fig. 4) show that the numerical solution fits well with the analytic potential (see Appendix). The maximum relative error is less than 0.15 per cent in S2. As to the potential profile in S1, the relative errors are less than 0.40 per cent when the observation points are more than 15 m away from the source, but a sharp increase appears in close

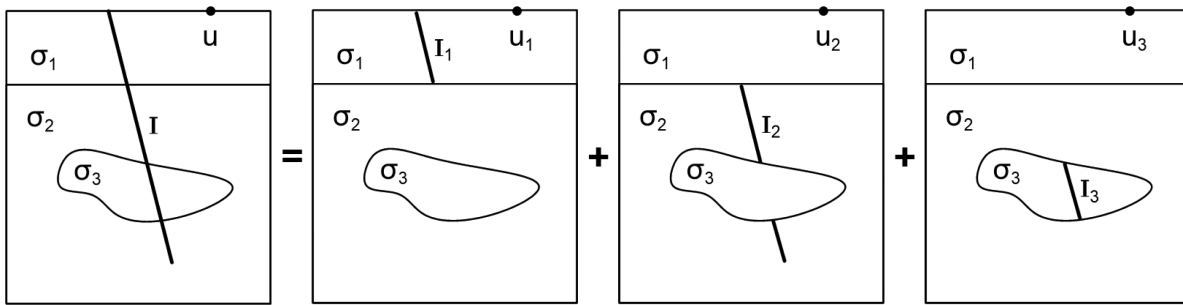


Figure 2. Schematic diagram of LE decomposition in heterogeneous media when secondary-potential method is applied for the simulation.

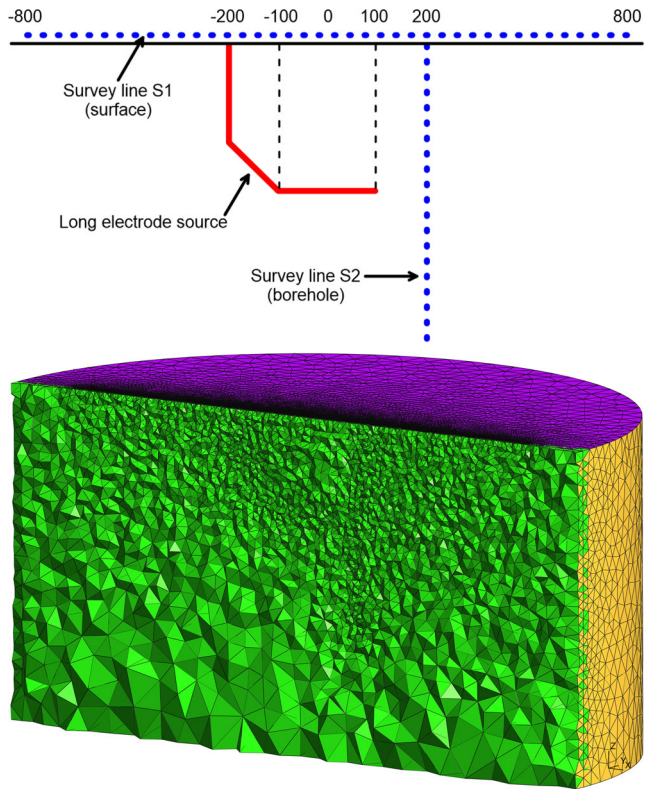


Figure 3. (a) Schematic illustration of a three-sectioned LE source in a homogeneous half-space. (b) Unstructured tetrahedral meshes of the model.

proximity to the top end of the source with the maximum relative error reaching 1.80 per cent at a distance of 5 m from the LE. Such fluctuation occurring in the vicinity of the source results from the singularity of the source and cannot be eliminated for total-potential method.

The potential distribution in the $x-z$ plane ($y = 0$) (Fig. 5a) shows a unique radiation pattern of LE source, differing from a PE source. The difference between a PE and LE sources implied from the contour plot is that a PE acts like an incandescent lamp that focuses the current at one point and radiates in all directions while the LE ‘lights’ an area almost uniformly like a fluorescent tube. Consequently, more current flow may be injected into greater depth. The equipotential surface of the electrical field excited by the LE source is similar to that by a ground PE source when the observation point is far enough away, typically two or three times the size of the LE. The relative errors between the numerical and analytic solutions on the $x-z$ plane are less than 0.5 per cent except in the vicinity of the source line (Fig. 3b).

3.2 A two-layer model for secondary-potential method

To analyse the accuracy of the secondary-potential-version FE algorithm, we design a two-layer model with an LE source inserting vertically into the cover layer (Fig. 6a). Both secondary-potential- and total-potential-version FE algorithms are applied to the simulation and the simulation results are compared with the analytic solution. The total potential profiles obtained by total-potential and secondary-potential methods are both in good agreement with the analytic solution (Fig. 6b). However, if the secondary potential is separated from the total potential, increasing deviation appears in the secondary potential profile obtained by total-potential method when approaching the source (Fig. 6c). For secondary-potential method, on the other hand, high computational accuracy is shown throughout the whole profile as the singularity of the source is removed.

Ronczka *et al.* (2015) discussed the apparent resistivity of LE arrays, in which the geometric factors are calculated numerically using CEM simulation. We offer another method for calculating the apparent resistivity of LE arrays. According to the analytic solution of the half-space model, the geometric factor of a pole-pole LE array reads (see Appendix)

$$k = \frac{4\pi L}{F_1 + F_2}, \quad (23)$$

where L is the length of the LE while F_1 and F_2 are coefficients related to the geometry of the LE and the field location. With eq. (23), the apparent resistivities formulas of common survey arrays as defined for PE sources, such as pole–pole, pole–dipole, dipole–pole, dipole–dipole, can be applied to arrays with LE sources. However, when a pair of LEs is used as the positive and negative poles, it may not be appropriate to name it a dipole source from the physical point of view, because the length of the LE source is not negligible. In this study, a pair of LEs for current injection is called a bipolar source, regardless of the electrode spacing. Although PEs are employed as measuring electrodes, we still use the term bipolar for a pair of measuring PEs for consistency consideration. The analytic and numerical $1/k$ profiles of pole–pole LE array are compared with the one of PE array (Fig. 7). To obtain the numerical $1/k$ profile, we implement a 3-D simulation algorithm for the electrical field of PE sources using FEM on unstructured tetrahedral grids. The algorithm is used to calculate the CCM approximation and then we follow the method of Ronczka *et al.* (2015) to obtain the geometric factor numerically. Obviously, the analytic and numerical profiles are matched and both deviate from the PE profile gradually when approaching the source.

The ground apparent resistivity profiles of pole–pole, pole–bipole, bipolar–pole and bipolar–bipole arrays with ground PE and vertical LE sources in the two-layer model are compared in Fig. 8. The ρ_a^{PP} profile shows the actual resistivity of the cover layer in small offset in the case of a PE source, but the profile with an LE

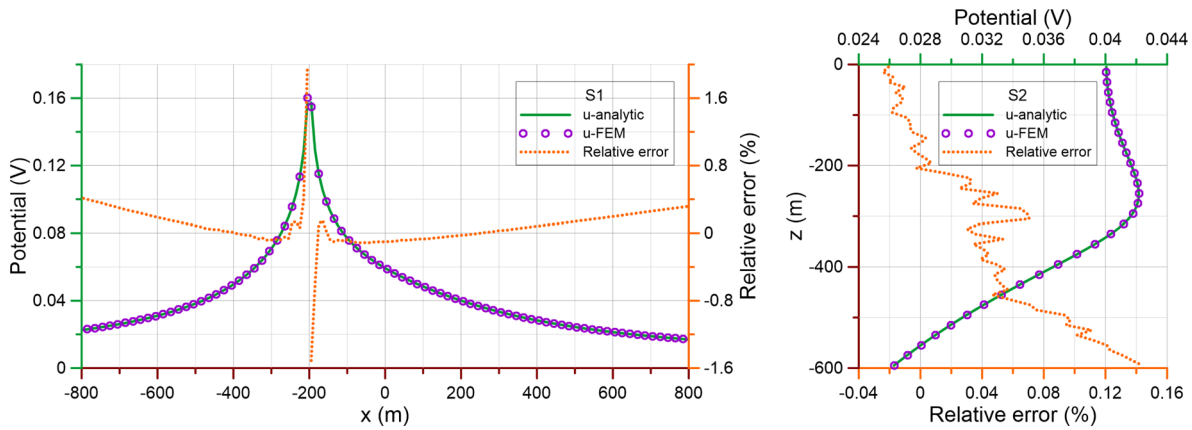


Figure 4. Numerical, analytical potential profiles and relative errors along survey lines S1 (left) and S2 (right).

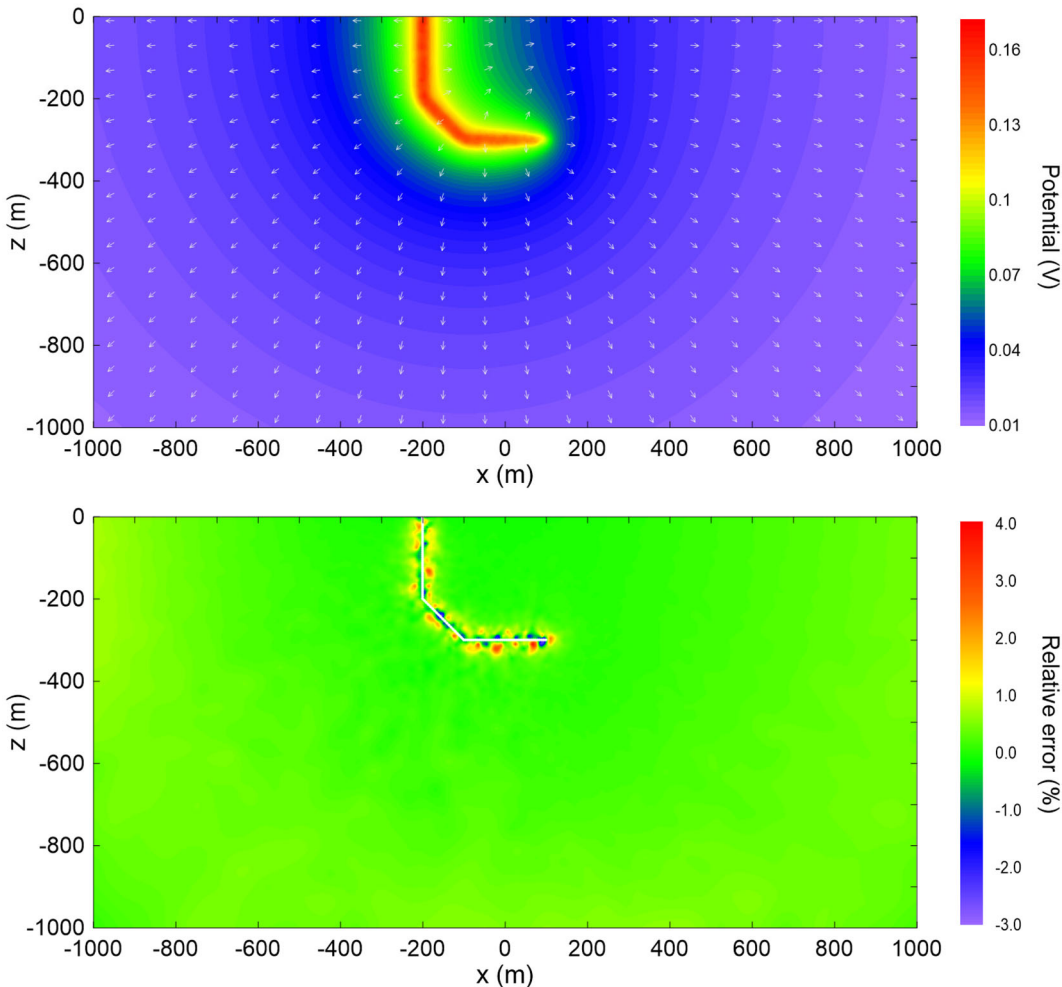


Figure 5. (a) Potential distribution on the x - z plane ($y = 0$) that the long electrode lies in. The white arrows depict the path of the current flow. (b) Relative error distribution on the plane.

source does not reach the actual resistivity at small offset while the resistivity of the base layer is shown at large offset. The length extent of the LE should account for the deviation in small offset. The ρ_a^{PB} , ρ_a^{BP} and ρ_a^{BB} profiles with the LE sources, however, show the resistivity of the two layers at small and large offsets respectively, the same as those of the PE source arrays, which demonstrate the practicability of our apparent resistivity formulas.

3.3 LE passing through heterogeneous media

We have introduced the CDA equation (10) for calculating the current density along an LE source penetrating through heterogeneous media, but it is difficult to verify the accuracy of the CDA equation analytically. In this section, our FEM algorithm with CDA correction is applied to the three-layer model used by Zhang *et al.* (2014) in which an 800 m long vertical LE source penetrates through all

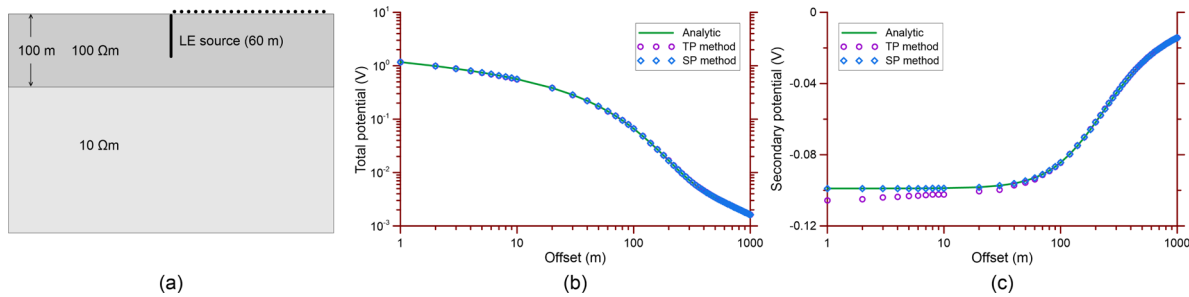


Figure 6. (a) A horizontal two-layer model with an LE source. The LE source is inserted into the cover layer vertically. (b) Total potential profiles. (c) Secondary potential profiles.

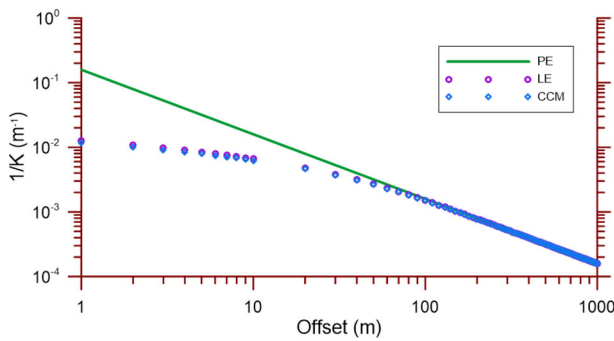


Figure 7. Geometric factors of pole-pole LE array obtained analytically (solid green line) and numerically (dashed blue line) and pole-pole PE array (dotted orange line).

three layers. The resistivities of the layers are 30, 10 and 30 Ωm from top to bottom and the thickness of the upper two layers is 300 m. The current density and potential profiles in four vertical boreholes with offsets of 2.5, 10, 25 and 50 m are compared with the CCM and non-CDA correction results (Fig. 9). In the CCM mesh model, a vimineous cylinder with a radius of 0.5 m and a resistivity of 10^{-6} Ωm is placed at the source location and energized by a point source on top. Obviously, the simulation results without CDA correction are not reliable. The solution with CDA correction, on the other hand, is consistent with the CCM solution in the upper two layers, but increasing deviations are shown towards the bottom end of the electrode at small offset. The fact that our model neglects the resistivity of the electrode may account for this deviation. The deviation becomes inconspicuous when the offset is larger than 25 m in the potential profiles (Figs 9c and d). Thus the CDA equation provides a good approximation to the real current density distribution and our simulation with the CDA correction is able to provide accurate result when the region of interest is not extremely close to the bottom end of the electrode.

We need to point out that our simulation with the CDA correction is more efficient than the CCM. For CCM, the mesh model is more complicated and more tetrahedral elements are to be generated due to the presence of the slim cylinder. Our model, on the other hand, does not require such a cylinder and the degree of freedoms in the model is largely reduced under the same mesh size setting. Furthermore, the SSOR-PCG solver fails to reach a convergent solution at maximum iteration steps for CCM due to the sharp resistivity contrast between the highly conductive cylinder and the surrounding earth media which results in an ill-conditioned system. Even with the direct solver, the solution is still not smooth enough in source region (Fig. 9a). Detailed comparisons regarding efficiency between the CCM and our model are listed in Table 1. To sum up,

our FEM algorithm is efficient and reliable for the simulation with arbitrary LE sources.

4 NUMERICAL EXAMPLES

4.1 Ground survey

Wastewater injected into the ground illegally by chemical factories has caused severe underground water pollution in China. electrical resistivity survey is an effective method for detecting the pollution area and monitoring the flow direction of the contaminated fluid. A simplified model of underground wastewater injection is designed (Fig. 10) for 3-D simulation with both LE and PE sources in this section. The underground wastewater, injected through a 50 m long metal pipe, is in the shape of a flattened badminton with a thickness of around 8 m and central depth at 50 m. The wastewater is assumed to be highly conductive (0.75 Ωm) due to the heavy-metal solute and other chemicals within it and the background resistivity is 10 Ωm. The top end of the metal pipe locates at the origin (0, 0, 0) and 36 survey lines are set up radially on the ground, centring at the pipe. There are 39 measuring electrodes in each survey line and the electrode spacing is 5 m. Using the pipe as an LE source, we can simulate the potential distribution and calculate the apparent resistivities of pole-pole and pole-bipole arrays. For comparison, 3-D simulation with a PE source placed right on top of the pipe is also conducted, but the low resistivity pipe is removed in order to investigate the pure electrical field arisen from a PE source. The contours of ground apparent resistivity with both PE and LE sources show the actual direction of the wastewater flow with obvious resistivity anomalies lying towards x-axis (Fig. 11). Note that the colour scale is the same for the four subfigures and it is clear that the LE source arouses larger anomalous signal than the PE source in both pole-pole and pole-bipole arrays. We define the relative resistivity anomaly as $R_a = (\rho_a - \rho_p)/\rho_p \times 100$ per cent with ρ_a and ρ_p denoting the apparent and background resistivities, respectively. The maximum R_a obtained using the LE source is nearly twice of that with the PE source in both pole-pole and pole-bipole arrays (Table 2), which indicates that the electrical field evoked by an LE source is more sensitive to conductive anomalies than that of a PE source.

We also investigate the use of long electrode for potential measurement with this model. To do so, the survey line along x-axis which lies right above the wastewater area is chosen and the potential electrode is replaced by LEs. The simulation result (Fig. 12) shows that the long potential electrode collects larger anomalous signal than the ground PE and the longer LEs are better than the shorter ones for potential measurement. At the right end of the apparent resistivity profile, we can also recognize the artificial anomaly

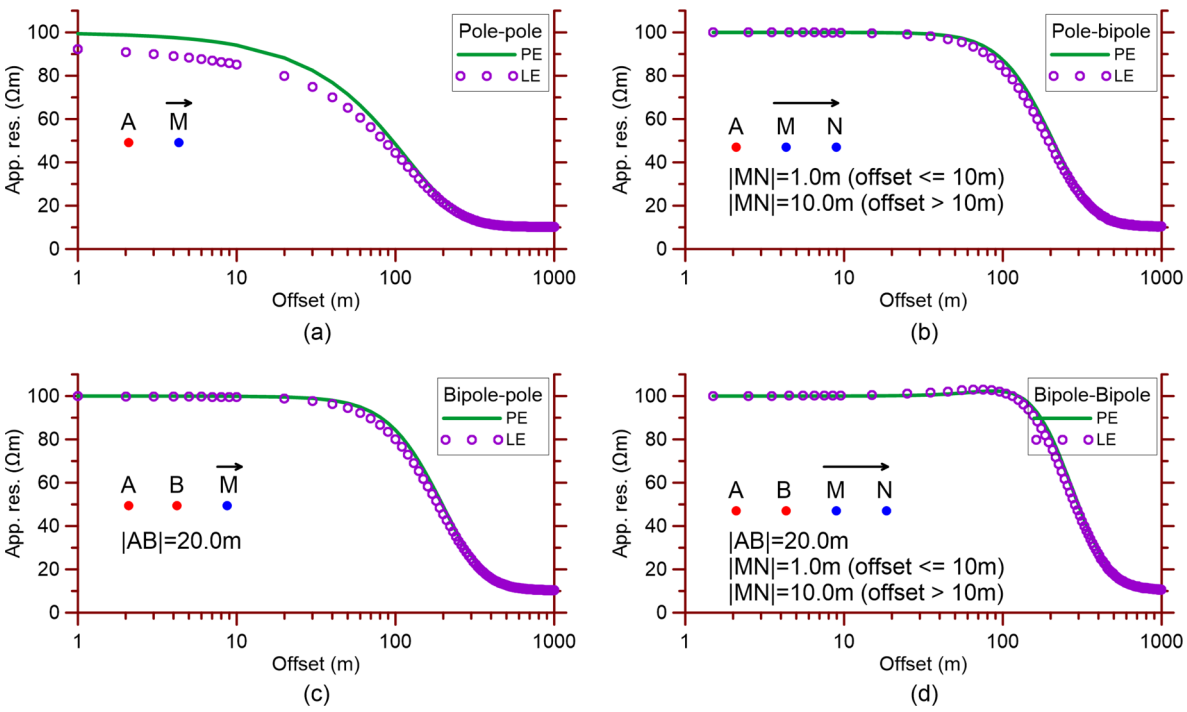


Figure 8. Apparent resistivity profiles of Pole–pole (a), pole–bipole (b), bipole–pole (c) and bipole–bipole (d) arrays with LE and PE sources.

aroused by the highly conductive LEs themselves and such artificial anomaly should be corrected when the data is used for geological interpretation. Although long potential electrodes are superior for identifying underground anomalies laterally, they are lacking in vertical resolution (Daily *et al.* 2004; Rucker *et al.* 2011). For quantitative interpretation, ground or borehole data collected by PEs are needed to recover the vertical resolution.

4.2 Borehole survey

Similar to conventional electrical prospecting with PE sources, when it comes to targets in the deep, the useful signal evoked by the LE source may become weak on the ground. In order to detect objects at great depth, borehole data are preferred. A blind ore model (Fig. 13a) is designed to test the borehole application for the LE source. The cased wells CW1 and CW2 are drilled vertically and can be utilized as LE sources while BH1 is a borehole for observation. With these facilities, we can inject current through CW1 and measure electrical potentials in BH1 to obtain apparent resistivity profiles of pole–pole and pole–bipole arrays, or use CW1 and CW2 as a bipolar source and obtain apparent resistivity profiles of bipole–pole and bipole–bipole arrays in BH1. Conventional electrical prospecting with moving PE arrays, including pole–pole, pole–dipole, dipole–dipole and Wenner, are also simulated in BH1 for comparison. The electrode spacing is set to be 5 m in all cases. With such electrode spacing, it can be expected that conventional moving PE arrays in BH1 can hardly collect any significant anomalous signal aroused from the blind ore, hence the simulation results are not shown here.

The LE arrays, on the other hand, record large anomalous signals when approaching the depth of the blind ore, especially for the bipole–bipole array (Fig. 13b). Significant anomalous signals may be collected by moving PE arrays with larger electrode spacing, but with the same measuring spacing, the advantage of the LE source is evident. Moreover, our numerical experiment shows that it takes

994 sec to calculate the apparent resistivity profiles of four moving PE arrays, while for the LE arrays, the simulations are done in 8 s using the same meshes.

Through the comparison in ground and borehole simulations, we can draw the conclusion that the electrical fields excited by LE sources are more sensitive to the resistivity anomalies than those by PE sources. LE arrays are able to collect anomalous signal with higher signal to noise ratio. Many other numerical examples of LEs have been studied (Rücker & Günther 2011; Zhu & Feng 2011; Zhang *et al.* 2014; Johnson & Wellman 2015; Ronczka *et al.* 2015; Weiss *et al.* 2016) and actual field applications have been carried out (Rucker *et al.* 2010, 2011), which indicates that the LE source is a powerful tool in electrical prospecting and can be applied in diverse geophysical explorations. When cased wells, metal pipes or other facilities that can be used for current injection are available, it is a good choice to use these facilities as LE sources for electrical prospecting.

4.3 Time-lapsed monitoring

Hydrofracturing technique has been used in oil field for improving production efficiency in tight rock formations. Monitoring the hydraulic fracturing and assessing the saturation of residual oil are among the most attractive applications for electrical prospecting with LE sources in oil field. In this section, we are going to investigate the capability of the LE arrays for monitoring the hydraulic fracturing process using an oil reservoir model with a two-stage hydrofracturing (Fig. 14a). The model consists of three layers with rugged layer interfaces. The cover layer is about 105 m thick while the thickness of the second layer ranges from 180 m to 300 m. The central depth of the reservoir is about 1100 m. Two irregular hexahedra with volumes of around $100 \times 100 \times 100 \text{ m}^3$ are placed in the reservoir to represent the fracture zones generated by hydrofracturing and filled with conductive proppants (Fig. 14b). The resistivity of the proppant can be as low as $3 \times 10^{-4} \Omega\text{m}$ (Pardo &

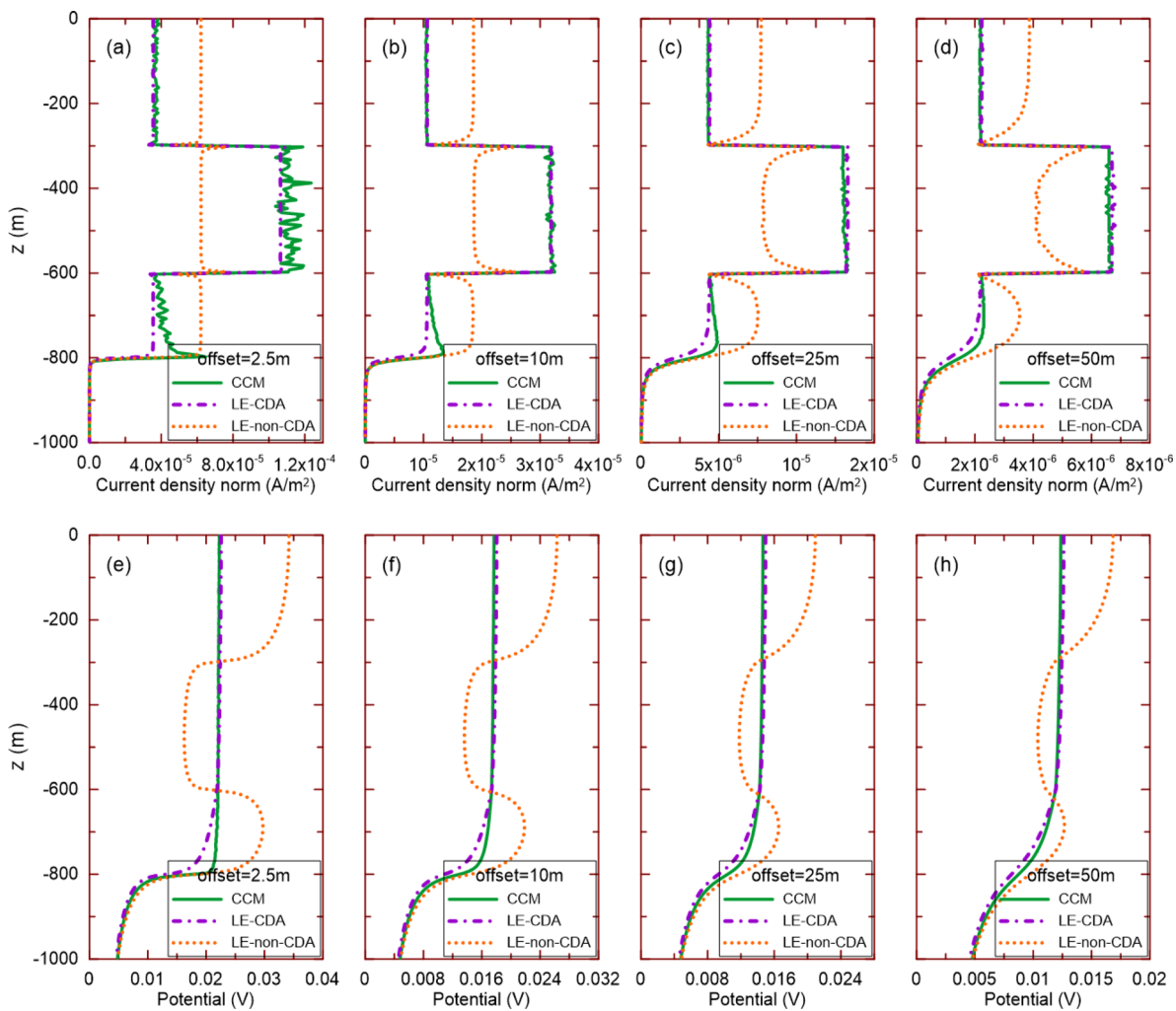


Figure 9. (a–d) Current density and (e–h) potential profiles in boreholes with offset = 2.5, 10, 25 and 50 m.

Table 1. Simulation efficiency with the CCM and CDA approximations.

Model	Tetrahedra	Nodes	SSOR-PCG iteration	SSOR-PCG time cost (s)	Pardiso time cost (s)
CCM	1 963 982	332 685	>5000	>412	9.98
LE-CDA	617 507	102 851	177	3.74	2.37

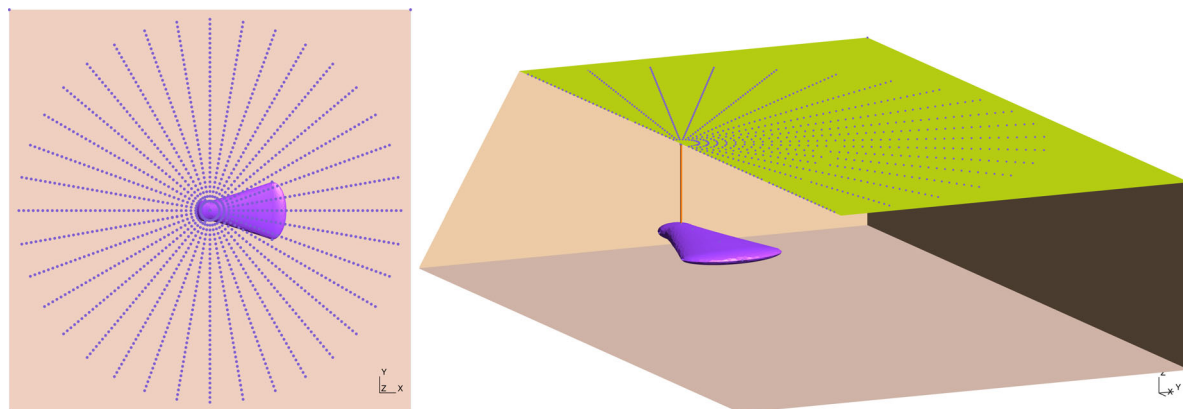


Figure 10. Top view (a) and side view (b) of a underground wastewater injection model.

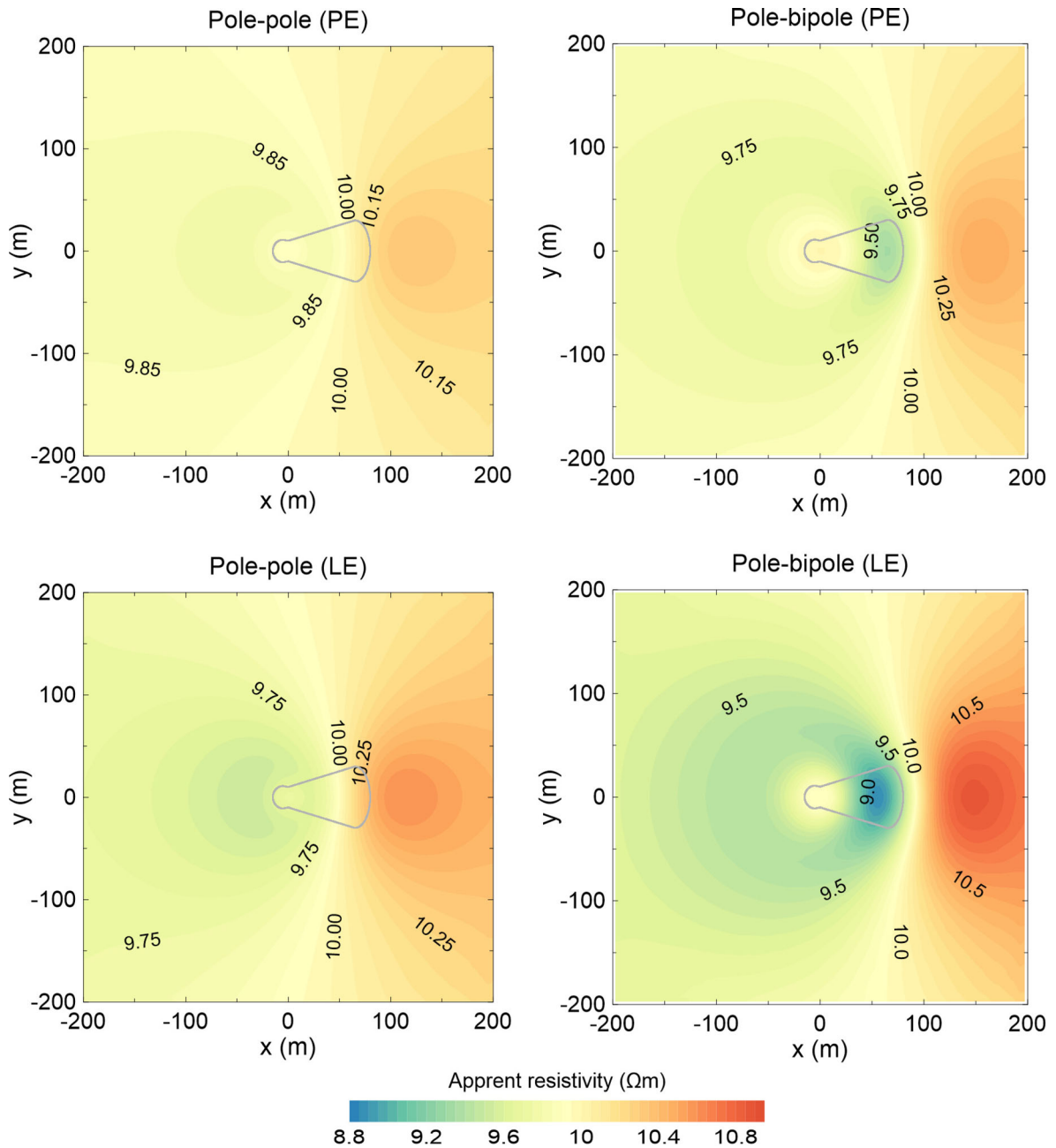


Figure 11. Contours plots of apparent resistivity of pole–pole and pole–bipole arrays with the PE and LE sources. The grey line depicts the horizontal location of the wastewater body.

Table 2. Maximum R_a in pole–pole and pole–bipole arrays.

Array	Pole–pole	Pole–bipole
PE source	3.39 per cent	−6.56 per cent
LE source	6.00 per cent	−11.41 per cent

Torres-Verdín 2013), but when the effective resistivity of multiphase media is considered (Yu & Wu 2010), the resistivity of the fracture system should be higher and 1 Ωm is assumed in this simulation. CW1, consisting of two casing sections, and CW2, a vertical cased well, are used as a bipolar LE source with an injection current of 15 A. At the beginning (Stage 0), no hydraulic fracture is generated, thus the resistivity of the fracture zones is the same as the oil reservoir (500 Ωm). The effective resistivity 1 Ωm is assigned to fracture

zone 1 in Stage 1 and then both fracture zones 1 and 2 are assigned 1 Ωm in Stage 2 to mimic the time-lapsed hydrofracturing process.

Potential difference (Δu) profiles with an electrode spacing of 10 m are collected in observation boreholes BH1–BH6 (Figs 15a–f). Maximum Δu appear in BH4 in Stage 1 (Fig. 15d), which is induced by fracture zone 1 right below it. In Stage 2, large Δu are shown in both BH3 (Fig. 15c) and BH4 (Fig. 15d), which reflects that a new fracture zone has been generated near BH3, other than fracture zone 1. Accordingly, LE arrays can be used for evaluating the location of the hydraulic fractures qualitatively.

In order to separate the pure anomalous signals corresponding to the fractures generated in different stages, we subtract the potential data of the former stage from those of the current stage and obtain the residual potential. The residual potential contours in the

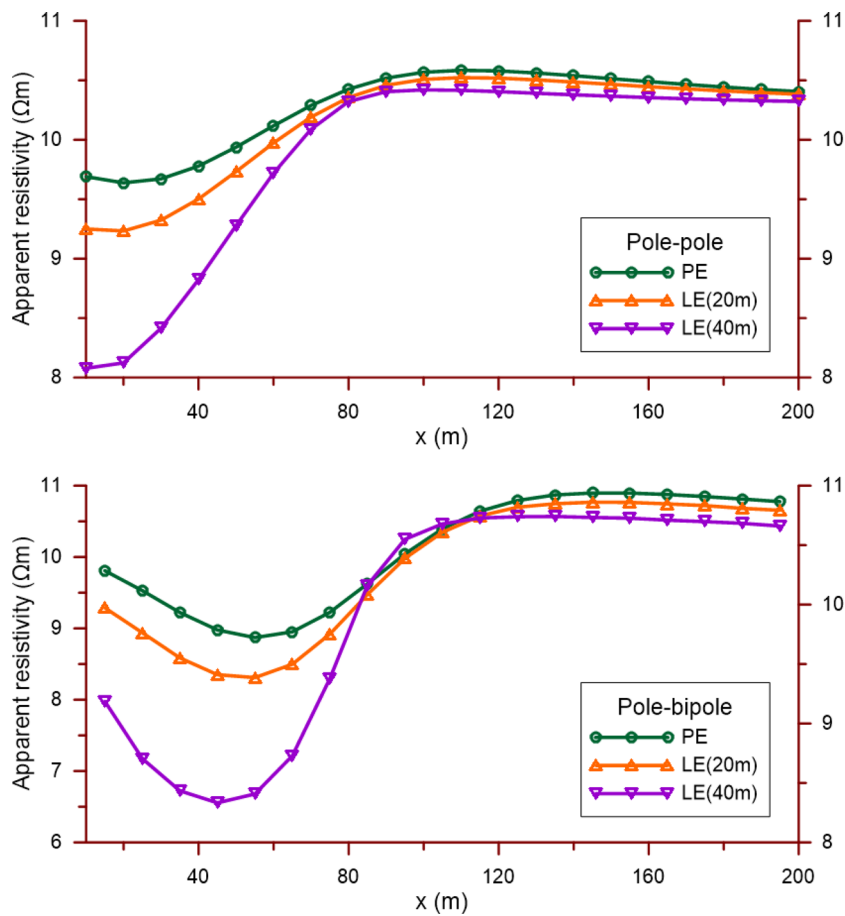


Figure 12. Apparent resistivity profiles with PEs, 20 m long and 40 m long LEs for potential measurement.

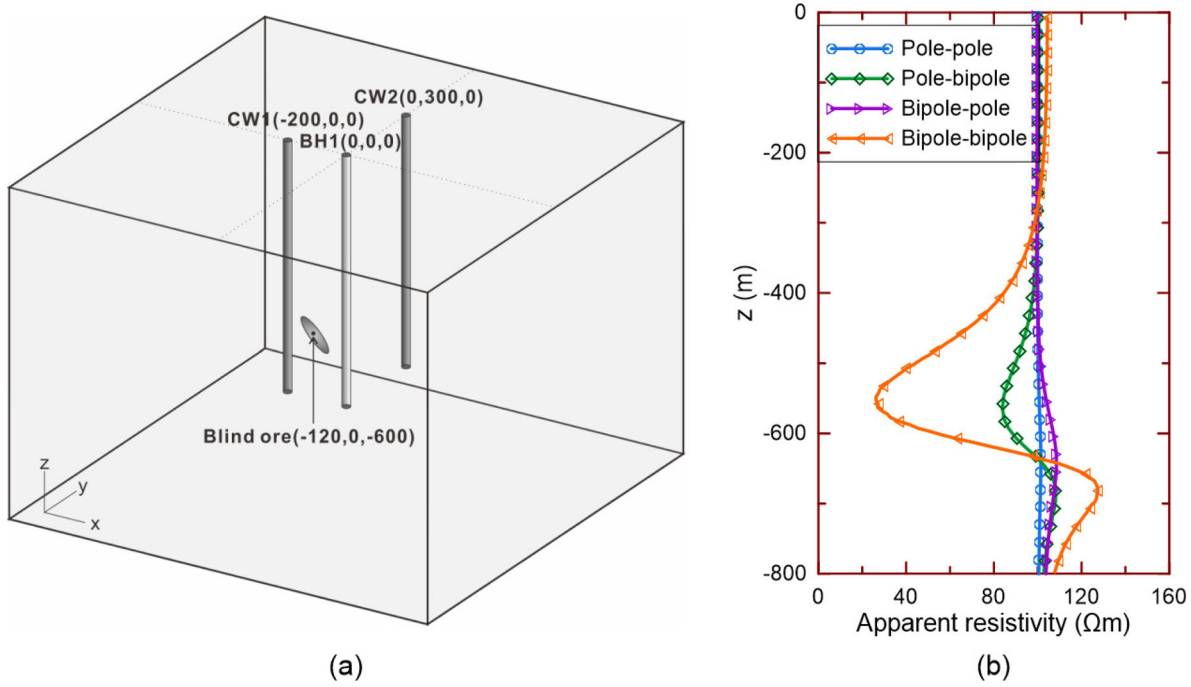


Figure 13. (a) A simplified blind ore model. Three wells are drilled to 800 m depth vertically. The blind ore, in the shape of ellipsoid with $a = 50$ m (x -direction), $b = 30$ m (y -direction) and $c = 10$ m (z -direction), is placed at $z = 600$ m with a dip of 45° . The resistivity of the ore is $10 \Omega\text{m}$ and the background resistivity is $100 \Omega\text{m}$. (b) Apparent resistivity profiles in BH1.

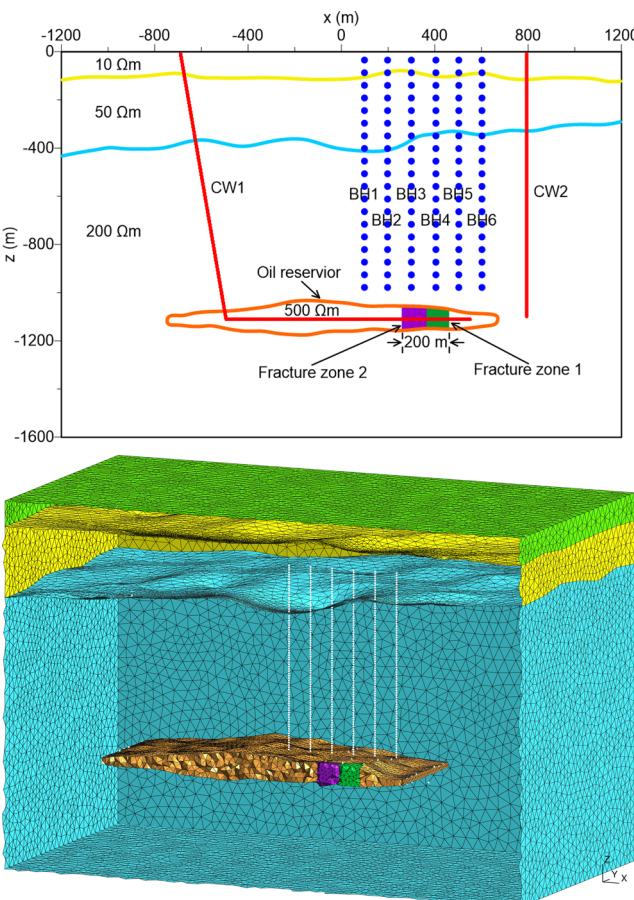


Figure 14. (a) Schematic of an oil reservoir model with a two-staged hydraulic fracturing zone (x - z plane cross-section at $y = 0$). (b) Meshes of the model (part). The white dotted lines represent the boreholes.

vertical plane $y = 0$ show a more clearer view of the hydrofracturing process in Stage 1 and 2 with maximum residual potential centred at the fracture zones (Fig. 16). The contour plots also imply that vertical survey lines are better choice for the time-lapsed monitoring as they are nearly perpendicular to the isolines of the residual potential and able to capture significant anomalous signals when the hydrofracturing is in progress. Compared with microseismic technology and other geophysical method, DC electrical prospecting is a low-cost, nondestructive, efficient and effective tool for monitor-

ing the hydraulic fracturing process in oil field. In order to provide precise evaluation of the fracture location and other parameters of the reservoir, such as residual oil saturation, new data process technique for LE arrays should be tested and the LE array data can be better interpreted by combining data from microseismology and other methods.

5 CONCLUSION AND DISCUSSION

The LE can be utilized as an extension to the DC electrical prospecting besides the PE source but the 3-D simulation of LE sources are more difficult than the PE cases. We have developed a new algorithm for simulating the electrical field of arbitrary LE sources and both total- and secondary-potential methods are integrated in the algorithm. Beyond the algorithm, several theoretical aspects of the LE source are covered, including the analytic solutions of the half-space model, surface current density distribution and apparent resistivity.

Many algorithms have been developed for the LE simulation. CCM, CEM and immersed interface method take into account the shape and size of the LEs in the simulation and thus they require a geometric representation of the LE in the mesh model. The existence of a slim LE in the model leads to a rapid increase in the number of elements during mesh generation, which results in high storage demand and low computational efficiency. Meanwhile, it is difficult to generate the meshes when an arbitrarily shaped LE with a small radius (e.g. 0.1 m) is placed in a large layered earth model (e.g. $1 \times 1 \times 1 \text{ km}^3$). If the radius of the LE is enlarged in the mesh model, significant numerical errors may occur in the simulation (Ronczka *et al.* 2015) and a trade-off between accuracy and computational effort is required. SEM, on the other hand, neglects the radius of the source and mimics the LE with a group of nodes connected via shunt conductors. Due to the line source assumption, SEM is easier to handle complicated LE sources. To achieve high accuracy, local refinement needs to be done along the LE, too. A remarkable advantage of SEM is that the potential electrode can also be represented by a group of nodes, which makes it convenient to simulate various LE arrays. CCM has been used as a reference model in literature, but no rigorous mathematical proof has been reported so far.

Our modelling scheme neglects both the radius and the resistivity of the LE, thus the shunting effect observed in the CCM result is not shown in our simulation. However, the comparison between our simulation and the CCM result shows that our algorithm is able to provide accurate numerical solution when the observation point is

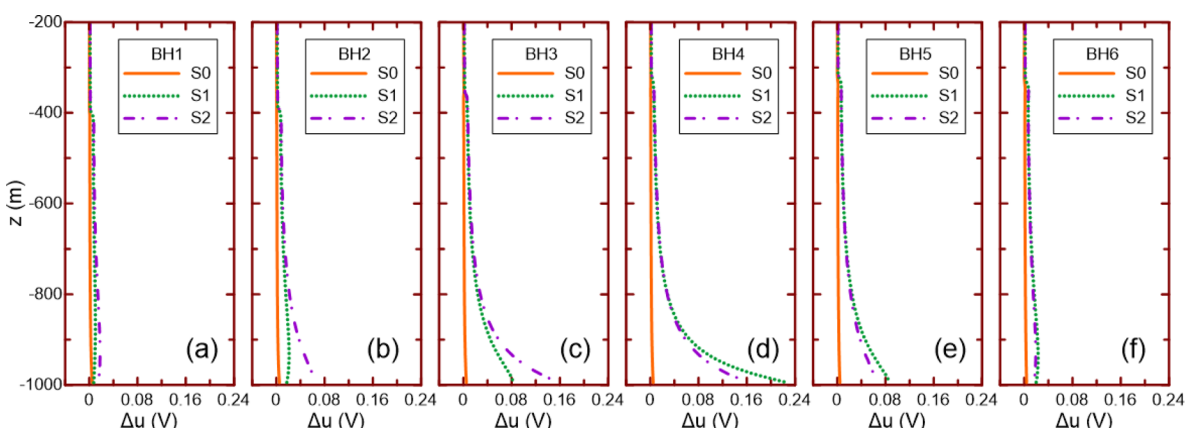


Figure 15. (a–f) Potential difference profiles of Stages 0 (S0), 1 (S1) and 2 (S2).

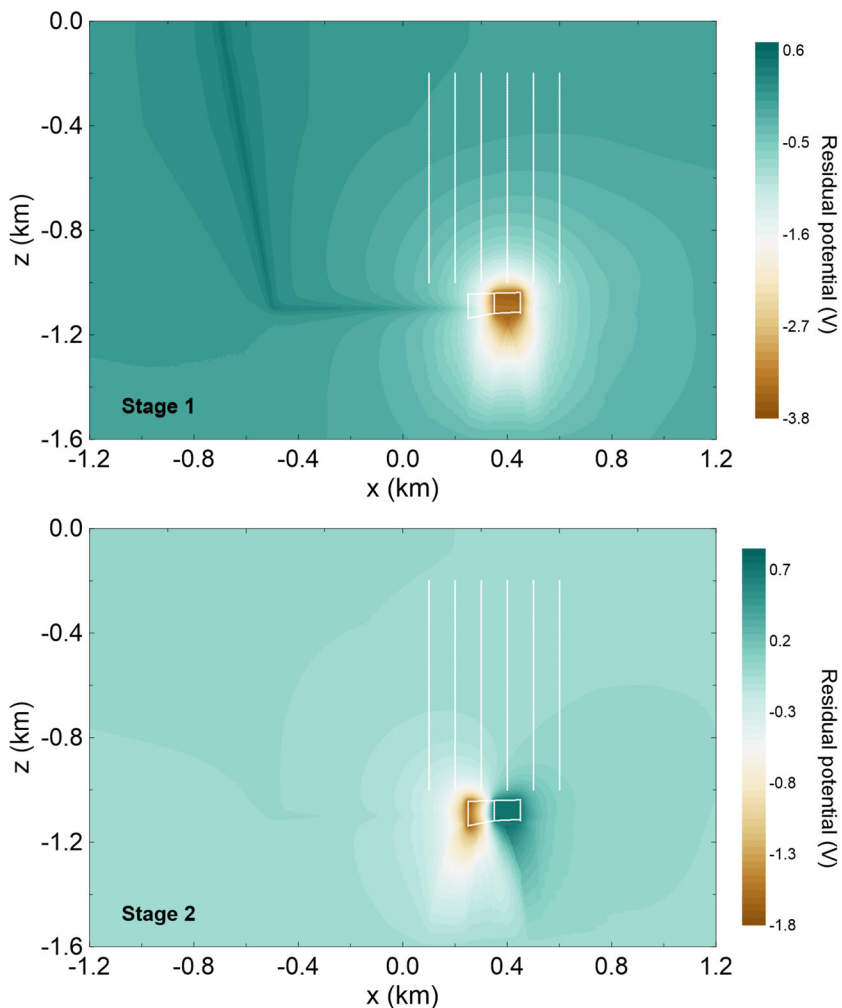


Figure 16. Residual potential contours in the vertical plane $y = 0$ at Stage 1 (a) and Stage 2 (b). The white dotted lines indicate the locations of the fracture zones and the survey lines in boreholes.

not extremely close to the bottom end of the electrode. Wells are usually hundreds of meters away from each other in oil field, thus the shunting effect of the LE can be neglected in the observation well and our CDA equation is able to provide good numerical approximations. Considering the practical field works, our algorithm is still a competitive solution for LE source simulation. First, our work extends the study of Zhu & Feng (2011) to arbitrarily multisected LE in heterogeneous conductive media by using an improved line source model which allows current strength allocation according to the surrounding resistivities. Second, our algorithm reduces the difficulty in mesh generation by abstracting the LE as a line source model. Third, secondary-potential method can be used in our simulation, but it is not applicable in CCM, CEM and SEM. In addition, the geometric factor k can be calculated analytically, rather than numerically, to obtain the apparent resistivity of LE arrays in our simulation.

More theoretical works still need to be done to investigate the shunting effect and improve the simulation result. Our future work will also include the development of inversion algorithm for the LE arrays. Although the resistivities of the surrounding media need to be determined first to implement the inversion using our LE model, fortunately, there are usually available resistivity logging data in oil field which can be used to solve the problem. Diverse applications are yet to be discovered with more field works.

ACKNOWLEDGEMENTS

J. Yang and Y. Liu are the co-first authors in this work. The paper is sponsored by the National Natural Science Foundation of China (41674076, 41130420, and 41374076), the National High Technology Research and Development Program of China (863 Program) (2012AA061403 and 2012AA09A201) and the Special-funded programme on national key scientific instruments and equipment development (2011YQ 05006008).

REFERENCES

- Beff, L., Günther, T., Vandoorne, B., Couvreur, V. & Javaux, M., 2013. Three-dimensional monitoring of soil water content in a maize field using electrical Resistivity Tomography, *Hydrol. Earth Syst. Sci.*, **17**, 595–609.
- Beresnev, I.A. & Atkinson, G.M., 1997. Modeling finite-fault radiation from the ω^n spectrum, *Bull. seism. Soc. Am.*, **87**, 67–84.
- Bhagwan, J. & Troffimenkoff, F.N., 1982. electrical drill stem telemetry, *IEEE Trans. Geosci. Remote Sens.*, **20**, 193–197.
- Byun, J., Yu, J. & Seol, S.J., 2010. Crosswell monitoring using virtual sources and horizontal wells, *Geophysics*, **75**, SA37–SA43.
- Coggon, J., 1971. Electromagnetic and electrical modeling by the finite element method, *Geophysics*, **36**, 132–155.
- Daily, W., Ramirez, A., LaBrecque, D. & Nitao, J., 1992. electrical resistivity tomography of vadose water movement, *Water Resour. Res.*, **28**, 1429–1442.

- Daily, W., Ramirez, A., Newmark, R. & Masica, K., 2004. Low-cost reservoir tomographs of electrical resistivity, *Leading Edge*, **23**, 472–480.
- Geuzaine, C. & Remacle, J.F., 2009. Gmsh: a three-dimensional finite element mesh generator with built-in pre- and post-processing facilities, *Int. J. Numer. Methods Eng.*, **79**, 1309–1331.
- Hauck, C., 2002. Frozen ground monitoring using DC resistivity tomography, *Geophys. Res. Lett.*, **29**, 12-1–12-4.
- Israil, M. & Pachauri, A., 2003. Geophysical characterization of a landslide site in the Himalayan foothill region, *J. Asian Earth Sci.*, **22**, 253–263.
- Johnson, T.C. & Wellman, D., 2015. Accurate modelling and inversion of electrical resistivity data in the presence of metallic infrastructure with known location and dimension, *Geophys. J. Int.*, **202**, 1096–1108.
- Johnson, C.D., Swarzenski, P.W., Richardson, C.M., Smith, C.G., Kroeger, K.D. & Ganguli, P.M., 2015. Ground-truthing electrical resistivity methods in support of submarine groundwater discharge studies: examples from Hawaii, Washington, and California, *J. Environ. Eng. Geophys.*, **20**, 81–87.
- Li, Y. & Spitzer, K., 2002. Three-dimensional DC resistivity forward modelling using finite elements in comparison with finite-difference solutions, *Geophys. J. Int.*, **151**, 924–934.
- Lowry, T., Allen, M.B. & Shive, P.N., 1989. Singularity removal: a refinement of resistivity modeling techniques, *Geophysics*, **54**, 766–774.
- Maillol, J., Seguin, M.K., Gupta, O., Akhouri, H. & Sen, N., 1999. Electrical resistivity tomography survey for delineating uncharted mine galleries in West Bengal, India, *Geophys. Prospect.*, **47**, 103–116.
- Pardo, D. & Torres-Verdín, C., 2013. Sensitivity analysis for the appraisal of hydrofractures in horizontal wells with borehole resistivity measurements, *Geophysics*, **78**, D209–D222.
- Rocroi, J.P. & Koulikov, A.V., 1985. The use of vertical line source in electrical prospecting for hydrocarbon, *Geophys. Prospect.*, **33**, 138–152.
- Ronczka, M., Rücker, C. & Günther, T., 2015. Numerical study of long-electrode electrical resistivity tomography – accuracy, sensitivity, and resolution, *Geophysics*, **80**, E317–E328.
- Rücker, C. & Günther, T., 2011. The simulation of finite ERT electrodes using the complete electrode model, *Geophysics*, **76**, F227–F238.
- Rucker, D.F., 2012. Enhanced resolution for long electrode ERT, *Geophys. J. Int.*, **191**, 101–111.
- Rücker, C., Günther, T. & Spitzer, K., 2006. Three-dimensional modeling and inversion of dc resistivity data incorporating topography—I: Modeling, *Geophys. J. Int.*, **166**, 495–505.
- Rucker, D.F., Levitt, M.T. & Greenwood, W.J., 2009. Three-dimensional electrical resistivity model of a nuclear waste disposal site, *J. appl. Geophys.*, **69**, 150–164.
- Rucker, D.F., Loke, M.H., Levitt, M.T. & Noonan, G.E., 2010. Electrical-resistivity characterization of an industrial site using long electrodes, *Geophysics*, **75**, WA95–WA104.
- Rucker, D.F., Fink, J.B. & Loke, M.H., 2011. Environmental monitoring of leaks using time-lapsed long electrode electrical resistivity, *J. appl. Geophys.*, **74**, 242–254.
- Schenk, O. & Gärtner, K., 2004. Solving unsymmetric sparse systems of linear equations with PARDISO, *J. Future Gener. Comput. Syst.*, **20**, 475–487.
- Spitzer, K., 1995. A 3-D finite-difference algorithm for dc resistivity modelling using conjugate gradient methods, *Geophys. J. Int.*, **123**, 903–914.
- Sudha, K., Israil, M., Mittal, S. & Rai, J., 2009. Soil characterization using electrical resistivity tomography and geotechnical investigations, *J. appl. Geophys.*, **67**, 74–79.
- Ushijima, K., Mizunaga, H. & Tanaka, T., 1999. Reservoir monitoring by a 4-D electrical technique, *Leading Edge*, **18**, 1422–1424.
- Wait, J.R., 1982. *Geo-Electromagnetism*, pp. 1–67, Academic Press.
- Wang, T. & Hohmann, G.W., 1993. A finite-difference, time-domain solution for three-dimensional electromagnetic modeling, *Geophysics*, **58**, 797–809.
- Wang, W., Wu, X. & Spitzer, K., 2013. Three-dimensional DC anisotropic resistivity modeling using finite elements on unstructured grids, *Geophys. J. Int.*, **193**, 734–746.
- Ward, S.H. & Hohmann, G.W., 1987. Electromagnetic theory for geophysical applications, in *Electromagnetic Methods in Applied Geophysics*, vol. 1, chap. 4, pp. 131–311, ed. Nabighian, M.N., Soc. Expl. Geophys.
- Waters, G.A., Dean, B.K., Downie, R.C., Kerrihard, K.J., Austbo, L. & Mcpherson, B., 2009. Simultaneous fracturing of adjacent horizontal wells in the woodford shale. Paper SPE119635 presented at the SPE Hydraulic Fracturing Technical Conference, Woodlands, TX, USA, January.
- Weiss, C.J., Aldridge, D.F., Knox, H.A., Schramm, K.A. & Bartel, L.C., 2016. The direct-current response of electrically conducting fractures excited by a grounded current source, *Geophysics*, **81**, E201–E210.
- Wu, X., 2003. A 3-D finite-element algorithm for DC resistivity modelling using the shifted incomplete Cholesky conjugate gradient method, *Geophys. J. Int.*, **154**, 947–956.
- Yu, Y. & Wu, X., 2010. Study of the generalized mixture rule for determining effective conductivity of two-phase stochastic models, *App. Geophys.*, **7**, 210–216.
- Zhang, Y.Y., Liu, D.J., Ai, Q.H. & Qin, M.J., 2014. 3D modeling and inversion of the electrical resistivity tomography using steel cased boreholes as long electrodes, *J. appl. Geophys.*, **109**, 292–300.
- Zhao, S. & Yedlin, M., 1996. Some refinements on the finite-difference method for 3-D DC resistivity modeling, *Geophysics*, **61**, 1301–1307.
- Zhou, B. & Greenhalgh, S.A., 2001. Finite element three-dimensional direct current resistivity modeling: accuracy and efficiency considerations, *Geophys. J. Int.*, **145**, 679–688.
- Zhu, T., 2012. Reply to the comment by D.F Rucker ‘T. Zhu and R. Feng, Resistivity tomography with a vertical line current source and its applications to the evaluation of residual oil saturation’, *J. appl. Geophys.*, **86**, 162–163.
- Zhu, T. & Feng, R., 2011. Resistivity tomography with a vertical line source and its application to the evaluation of residual oil saturation, *J. appl. Geophys.*, **73**, 155–163.

APPENDIX: ELECTRICAL POTENTIAL IN HOMOGENEOUS HALF-SPACE WITH LE SOURCES

As shown in Fig. A1, an LE source **AB** is embedded in a homogeneous half-space ($z \leq 0$) with conductivity σ . The length of the LE is L and the total injection current is I . We denote the mirror image of the LE by **A'B'**. The LE can be divided into a series of line segments, and the potential at observation location P evoked by the line segment dl at point Q reads

$$du = \frac{Idl}{4\pi\sigma L} \left(\frac{1}{r} + \frac{1}{r'} \right), \quad (\text{A1})$$

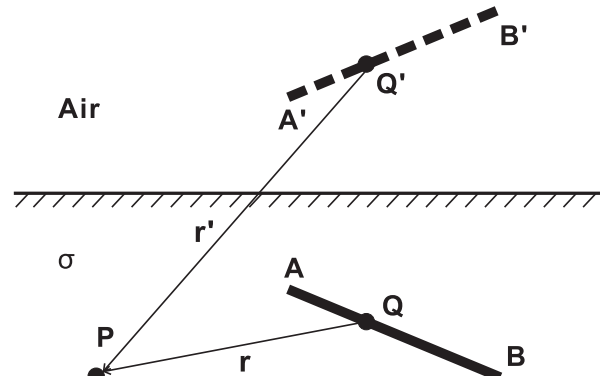


Figure A1. Sketch of a long electrode in a homogeneous half-space

where $r = |\mathbf{QP}|$ and $r' = |\mathbf{Q}'\mathbf{P}'|$. Since the potential u is a scalar field, the total potential evoked by the whole LE can be obtain by integrating eq. (A1) along the source line L ,

$$u = \frac{I}{4\pi\sigma L} \int_L \left(\frac{1}{r} + \frac{1}{r'} \right) dl. \quad (\text{A2})$$

As $\mathbf{QP} = \mathbf{AP} - \mathbf{AQ} = \mathbf{AP} - t\mathbf{AB}$, $t \in [0, 1]$, then

$$r = |\mathbf{QP}| = \sqrt{\mathbf{AB}^2 t^2 - 2\mathbf{AB} \cdot \mathbf{AP}t + \mathbf{AP}^2}. \quad (\text{A3})$$

Likewise, we have

$$r' = |\mathbf{Q}'\mathbf{P}'| = \sqrt{\mathbf{A}'\mathbf{B}'^2 t^2 - 2\mathbf{A}'\mathbf{B}' \cdot \mathbf{A}'\mathbf{P}'t + \mathbf{A}'\mathbf{P}'^2}. \quad (\text{A4})$$

Let

$$\begin{aligned} a &= \mathbf{AB}^2, & b &= -2\mathbf{AB} \cdot \mathbf{AP}, & c &= \mathbf{AP}^2, \\ a' &= \mathbf{A}'\mathbf{B}'^2, & b' &= -2\mathbf{A}'\mathbf{B}' \cdot \mathbf{A}'\mathbf{P}', & c' &= \mathbf{A}'\mathbf{P}'^2, \end{aligned} \quad (\text{A5})$$

and eqs (A3) and (A4) become

$$r = \sqrt{at^2 + bt + c}. \quad (\text{A6})$$

$$r' = \sqrt{a't^2 + b't + c'}. \quad (\text{A7})$$

To simplify the integral in (A2), we split the integrand into two parts and denote them by

$$F_1 = \int_L \frac{1}{r} dl, \quad (\text{A8})$$

$$F_2 = \int_L \frac{1}{r'} dl. \quad (\text{A9})$$

With eq. (A6), variable substitution can be applied to (A8) and F_1 becomes

$$F_1 = \int_0^1 \frac{L dt}{\sqrt{at^2 + bt + c}}. \quad (\text{A10})$$

Integral (A10) is conditionally convergent and finally we have

$$F_1 = \begin{cases} \ln \frac{2a + b + 2\sqrt{a(a + b + c)}}{b + 2\sqrt{ac}}, & 4ac - b^2 > 0, \\ \ln \frac{b}{2a + b}, & 4ac - b^2 = 0, b < 0, \\ \ln \frac{2a + b}{b}, & 4ac - b^2 = 0, b \geq 0. \end{cases} \quad (\text{A11})$$

Similarly, integral (A9) gives

$$F_2 = \begin{cases} \ln \frac{2a' + b' + 2\sqrt{a'(a' + b' + c')}}{b' + 2\sqrt{a'c'}}, & 4a'c' - b'^2 > 0, \\ \ln \frac{b'}{2a' + b'}, & 4a'c' - b'^2 = 0, b' < 0, \\ \ln \frac{2a' + b'}{b'}, & 4a'c' - b'^2 = 0, b' \geq 0. \end{cases} \quad (\text{A12})$$

Finally, the electrical potential evoked by an arbitrary LE source embedded in a homogeneous half-space reads

$$u = \frac{1}{k} \rho I, \quad (\text{A13})$$

where

$$k = \frac{4\pi L}{F_1 + F_2} \quad (\text{A14})$$

is the geometric factor for LE source and the resistivity $\rho = 1/\sigma$. We need to point out that eq. (A2) holds for arbitrary line path, so eq. (A13) can also be used for calculating the electrical potential evoked by arbitrarily multisected LE sources.